JOURNAL OF THERMOPHYSICS AND HEAT TRANSFER
Vol. 7, No. 2, April–June 1993

Flowfield Coupled Excitation and Radiation Model for Nonequilibrium Reacting Flows

Thomas A. Gally,* Leland A. Carlson,† and Derek Green‡
Texas A&M University, College Station, Texas 77843

A second-order method has been developed to correct a radiative transfer analysis for possible local thermodynamic nonequilibrium effects. This method uses a two-species excitation model for nitrogen with chemical reaction rates obtained from the detailed atomic transition method of Kunc and Soon. Results obtained from this new method show more atomic line radiation than the authors' previous first-order method. As improvements to the flowfield representation used in the computations, a full three-temperature energy model and a recently developed multicomponent diffusional model have also been incorporated.

Nomenclature

B_ν = blackbody function
c = speed of light
c_p = specific heat at constant pressure
E = electronic state energy level
E_n = integro-exponential function of order n
e = energy per unit mass
g = degeneracy
h = enthalpy per unit mass
I = ionization energy
K = absorption coefficient
k = Boltzmann constant
m = particle mass
N = number density
p = pressure
Q = electronic partition function
Q_e = electron translational partition function
q_r = radiative heat flux
r = wall reflectivity
S = source function
T = temperature
t = time
U = diffusion velocity
u^j = mass-averaged velocity components
x^j = coordinate axis
ε = wall emissivity
η = heat conduction coefficient
ν = frequency
ρ = density
σ = radiative cross section
τ = relaxation time
τ_ν = optical thickness

Subscripts

e = electron-electronic
f = forward rate (production)
pc = continuum process
pq = line process
r = reverse rate (depletion)
s = species
sh = value at shock
tr = translational
v = vibrational
w = value at wall
ν = frequency

Introduction

A GREAT deal of interest has been placed recently on the design of aerobraking vehicles for use with both interorbit maneuvering and interplanetary deceleration. In particular, a major goal of such experimental projects as the aeroassist flight experiment (AFE) is the development of the computational tools for the accurate prediction of the aerodynamic environment which determines the heating and controllability of such vehicles. Both low-speed interorbit and high-speed interplanetary missions will spend the aerobraking portion of their trajectories at very high, low-density altitudes where previously developed space vehicles spent only short durations. Thus, the computational aerodynamic tools to be used must correctly handle the chemical, thermal, and radiative nonequilibrium phenomena associated with low-density flows.

Previous work[1,2] concentrated on some aspects of the nonequilibrium nature of aerobraking flowfields. For example, the primary topic of discussion in Ref. 1 was electron-impact ionization rates. This chemical rate is important in both determining the amount of chemical nonequilibrium in the flow and in calculating the electron temperature T_e. Existing rates in the literature varied over several orders of magnitude with accompanying differences in T_e profiles and wall radiative heating rates, which is a strong function of T_e. In Ref. 2, the effects of thermodynamic nonequilibrium on the magnitude and nature of the radiative environment was investigated. Comparisons were made with the FIRE II flight test measurements, and a wide range of possible mission profile conditions were investigated.

A number of topics for future work were identified from the previous work. First, a two-temperature, T_{tr} and T_e, model had been used exclusively in Refs. 1 and 2, in which it was assumed that $T_v = T_{tr}$. This model is probably accurate for the higher speed conditions above 12 km/s where the flow is ionization-dominated and few diatomic particles exist. However, at the lower speeds and particularly for the speeds associated with the AFE vehicle, the flowfield is dissociation-dominated; and the inclusion of a separate vibrational energy equation can be expected to affect the total results. In addition, electron-vibrational coupling will affect the predicted T_e profile and, therefore, the radiative environment. Second, diffusional phenomena seemed to significantly affect chemical nonequilibrium and also the extent of atomic thermodynamic nonequilibrium. Since the diffusional model that was then

---

Presented as Paper 91-1463 at the AIAA 22nd Fluid Dynamics, Plasma Dynamics, and Lasers Conference, Honolulu, HI, June 24–26, 1991; received Aug. 12, 1991; revision received May 14, 1992; accepted for publication June 24, 1992. Copyright © 1991 by the American Institute of Aeronautics and Astronautics, Inc. All rights reserved.

*NASA Graduate Student Researcher. Student Member AIAA.

†Professor Aerospace Engineering. Associate Fellow AIAA.

‡Graduate Research Assistant.

being used was felt to be inadequate, a more complete model[3] has recently been incorporated into the flowfield solution. Finally, a new atomic local second-order thermodynamic nonequilibrium model was conceived, which is a compromise between the simple and fast method used previously and the complex methods used by other authors.

Problem Formulation

The computational model used in this report is an extension of the coupled viscous shock layer (VSL) and radiative transfer method described in detail in Refs. 1 and 2. The VSL portion of the code originated as the VSL3DNQ code[4] developed at NASA Langley. After modifications were made to the thermodynamic and transport coefficient calculations and multitemperature effects, T_{tr} and T_e, were included, the flowfield was iteratively coupled with the radiative transfer model of Nicolet[5] in a manner which included chemical and local thermodynamic nonequilibrium (LTNE) phenomena.

Three additional modifications have been made for this article. First, a vibrational energy equation has been added for the calculation of a third temperature, T_v, which describes the average vibrational energy state of all the diatomic species. Second, a new diffusional model has been developed to improve the calculation of the diffusional fluxes of mass and energy. Finally, to improve LTNE predictions, second-order radiative correction factors similar to those used in Refs. 1 and 2 have been developed for a two-step excitation model for atomic nitrogen.

Vibrational Temperature Model

The vibrational energy equation added to the VSL calculations has the following form for simple Cartesian coordinates:

$$\rho u^j c_{p_v} \frac{\partial T_v}{\partial x^j} = \frac{\partial}{\partial x^j}\left(\eta_v \frac{\partial T_v}{\partial x^j}\right) + \sum_s \rho_s U_s \frac{\partial h_{v_s}}{\partial x^j}$$
$$+ \sum_s \rho_s\, A\, \frac{[e_{v_s}(T_{\text{tr}}) - e_{v_s}]}{\tau_s} + \sum_s \rho_s \frac{[e_{v_s}(T_e) - e_{v_s}]}{\tau_{e,s}}$$
$$+ \sum_s (e_{v_s} - E_s)\left(\frac{\partial \rho_s}{\partial t}\right)_f - \sum_s (e_{v_s} - G_s)\left(\frac{\partial \rho_s}{\partial t}\right)_r \qquad (1)$$

In this equation, c_{p_v} is the frozen vibrational specific heat at constant pressure calculated from the species specific heats by $\Sigma_s\, c_{p_{v},s}\rho_s/\rho$; and the vibrational temperature T_v represents the average vibrational energy of all the diatomic species. While multiple vibrational temperatures are often used, one for each vibrating species, it can be argued[6] that the vibrational-vibrational energy exchange rates are not well modeled by available methods; and, thus, results with multiple vibrational temperatures may not be meaningful. In addition, for the results with a nitrogen-only gas presented in this report, there is only one dominant vibrator, N_2, the vibrational contribution from N_2^+ being small.

The translational-vibrational energy exchange model used is a modification of the nonpreferential CVDV model described in Refs. 7 and 8. The terms involved with the $T_{\text{tr}} - T_v$ coupling model are the third, fifth, and sixth on the right side of Eq. (1). The differences from the CVDV model first occur, in the calculation of the relaxation time τ_s. This relaxation time is that proposed by Park[9] which sums the relaxation time of Millikan and White,[10] τ_s^{MW}, with a high temperature correction factor such that

$$\tau_s = \tau_s^{MW} + (1/c_s \sigma_v N_s)$$

where c_s is the average species molecular speed and σ_v is a limiting cross section calculated by[11]

$$\sigma_s = 10^{-17}(50{,}000\ \text{K}/T_{\text{tr}})^2 \text{cm}^2$$

The second modification, also suggested by Park,[11] is the inclusion of the multiplier A on the third right-side term of Eq. (1). This multiplier attempts to correct the original Landau and Teller relaxation rate for high temperature diffusive effects and has the form

$$A = \left|\frac{T_{\text{tr,sh}} - T_v}{T_{\text{tr,sh}} - T_{v,\text{sh}}}\right|^{[3.5\ \exp(-5000\ \text{K}/T_v) - 1]}$$

The electron-vibrational energy exchange is accounted for by the fourth right-side term of Eq. (1) and is taken from the work of Lee[12] as curve-fitted by Candler and Park[13]

$$\log(p_e \tau_e) = 7.50(\log T_e)^2 - 57.0 \log T_e + 98.70$$

for $T_e < 7000$ K, and

$$\log(p_e \tau_e) = 2.36(\log T_e)^2 - 17.9 \log T_e + 24.35$$

for $T_e \geq 7000$ K.

Lee suggests a correcting factor for the electron-vibrational relaxation similar to the factor A used for translational-vibrational relaxation. As with the translation-vibrational relaxation factor, this term is intended to increase the relaxation time or decrease the amount of coupling between the electron energy and vibrational energy. Unfortunately, the form of the correction developed for the case was T_e and T_v, and being far apart initially has the opposite effect for our conditions where T_e and T_v are initially close together in value behind the shock. For this reason, the suggested correction has not been included in the present model and the calculated results may tend to show too much electron-vibrational coupling.

The electron-vibrational coupling factor must also be included in the electron temperature equation, which for this article is the full electron/electronic energy equation described in Ref. 2. The electron/electronic energy equation is similar in form to Eq. (1) and includes the effects of conduction, convection, diffusion, chemical energy depletion, heavy particle-electron translation coupling, and now electron-vibrational coupling.

Second-Order Atomic LTNE Model

The flowfield solution is coupled with the radiative transport package of RADICAL[5] developed by Nicolet. The methods used by Niclolet assume that the electronic states of the radiating species are in local thermodynamic equilibrium (LTE) with each other and that their populations can be described by a Boltzmann distribution. A technique was previously developed[1,2] for correcting the RADICAL calculations to account for LTNE in both the atomic and molecular state populations.

The molecular electronic states populations are calculated using a quasisteady approach similar to that described in Ref. 11; and from these, LTNE population correction factors for the principle molecular radiation bands are obtained. Specifically, correction factors are determined for the N_2 Birge-Hopfield, first-positive, and second-positive bands, and for the N_2^+ first-negative band. Reference 2 should be consulted for more detail.

Also discussed in Ref. 2 is a first-order atomic LTNE radiation correction. This model is predicated on the observation that for many monatomic gases, including argon, nitrogen, and oxygen, there exist one or more low-lying ground energy states separated from the lowest excited energy state by an energy jump which is a large fraction of the ionization energy from the ground state. The model assumes that the excitation jump from ground to first excited state controls the ionization process, and that the excited states, because of their proximity in energy to the ionized state, are in equilibrium with the free electrons and ions. With this approach, the atomic nitrogen LTNE correction factor,[1,2,14] which represents the ratio of the actual population in an excited state to that which would exist for a Boltzmann distribution, can be written as

$$\frac{N_{N^+}N_eQ_N \exp(169{,}000\ \mathrm{K}/T_e)}{N_NQ_{N^+}Q_e}$$

The above assumptions and resulting approximation are extremely simple to calculate and implement. At the other end of the spectrum are the methods of Park[9] and Kunc and Soon[15] which handle possible LTNE effects by performing detailed state population calculations under the quasisteady assumption. Park's and Kunc's methods differ in the treatment of the free electrons and ions; Kunc and Soon allow the free ions and electron populations to be determined as part of the solution, allowing LTNE to occur only as a consequence of radiative state depletion, while Park uses the ion and electron population calculated from the flowfield solution, allowing nonequilibrium chemistry to affect bound state populations. Either way, the detailed methods are computationally intensive and are not suitable for a radiative coupled solution if computational usage is a consideration.

After extensively reviewing the work on argon of Foley and Clarke[16] and Nelson,[17] and the air and nitrogen work of Park,[9] Kunc and Soon,[15] and others, it was decided to develop a second-order LTNE model for high-temperature nitrogen by subdividing atomic nitrogen into two species. The first, termed N_g, for N ground, represents the nitrogen atoms in the first three low-lying electronic states of nitrogen. The second, termed N* or N-excited, represents those nitrogen atoms populating the remaining upper electronic states. The relative densities of these subspecies will then be determined by appropriate reaction rates between themselves, N^+, e^-, etc., and the electronic states of each are assumed to be in LTE. It is believed that this approach has the potential to be a significant improvement over the present model in that it will allow a finite rate of ionization from excited states while retaining the fundamental two-step ionization process. In addition, by determining the excited state number densities directly from the flowfield computation, the appropriate atomic LTNE factors are directly obtainable and more accurate.

The thermodynamic state of the two species, N_g and N*, are determined by the standard methods used for monoatomic gases

$$Q_{\mathrm{N}_g} = \sum_{p=1}^{3} g_p \exp(-E_p/kT_e)$$

$$Q_{\mathrm{N}^*} = \sum_{p=4}^{\max} g_p \exp[-(E_p - E_4)/kT_e]$$

$$Q_{\mathrm{N}} = Q_{\mathrm{N}_g} + Q_{\mathrm{N}^*} \exp(-E_4/kT_e)$$

$$h_{\mathrm{N}_g} = \frac{5}{2}\frac{kT}{m_{\mathrm{N}}} + \frac{1}{m_{\mathrm{N}}Q_{\mathrm{N}_g}} \sum_{p=1}^{3} g_pE_p \exp(-E_p/kT_e) + h^\circ_{\mathrm{N}_g}$$

$$h_{\mathrm{N}^*} = \frac{5}{2}\frac{kT}{m_{\mathrm{N}}} + \frac{1}{m_{\mathrm{N}}Q_{\mathrm{N}^*}} \sum_{p=4}^{\max} g_p(E_p - E_4) \cdot \exp[-(E_p - E_4)/kT_e] + h^\circ_{\mathrm{N}^*}$$

where the zero point energies are, $h^\circ_{\mathrm{N}_g} = h^\circ_{\mathrm{N}} = 3.36 \times 10^{11}$ erg/g and $h^\circ_{\mathrm{N}^*} = h^\circ_{\mathrm{N}_g} + E_4/m_{\mathrm{N}} = 1.05 \times 10^{12}$ erg/g. The collision cross sections for both species, needed to calculate viscous transport properties, are assumed to be the same as for the original gas, N.

As mentioned earlier, new reactions must be specified to relate the two new species, N_g and N*. These reactions are

$$N_g + e^- = N^* + e^-$$

$$N_g + e^- = N^+ + 2e^-$$

$$N^* + e^- = N^+ + 2e^-$$

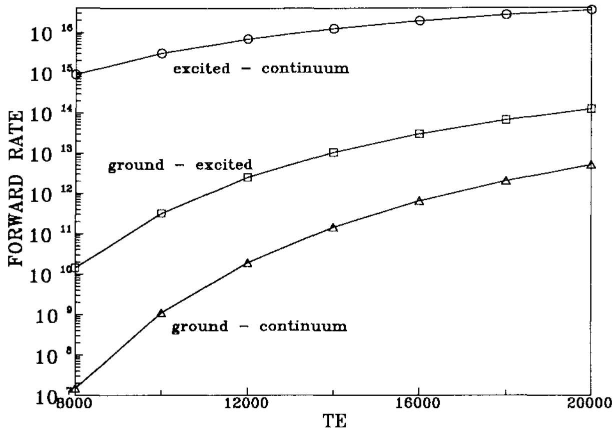

Fig. 1 Excitation and ionization rates for nitrogen-electron collisions.

It was decided to use the method for calculating detailed excitation rates given in Ref. 15. A computer program was written which calculated the individual rates for each allowed transition process and computed effective rates for the above reaction equations, assuming local thermodynamic equilibrium exists between the excited states grouped into each species. Results were obtained for a number of electron temperatures and then curve-fit as shown in Fig. 1. These rates are part of the complete chemical reaction set shown in Table 2.

The radiative transport model must also be modified to account for the LTNE populations of N_g and N* relative to each other. Under the assumption of a radiating tangent slab, the heat flux to a surface can be calculated as, assuming a nonemitting precursor

$$-q_{r_\nu}(x) = 2\pi \int_0^{\tau_{\nu,sh}} \mathrm{sgn}(t_\nu - \tau_\nu)S_\nu E_2(|t_\nu - \tau_\nu|)\, \mathrm{d}t_\nu - 2E_3(\tau_\nu)\pi \left[\varepsilon_w B_{\nu,w} - 2r_w \int_0^{\tau_{\nu,sh}} E_2(t_\nu)S_\nu\, \mathrm{d}t_\nu\right]$$

where τ_ν is determined by

$$\tau_\nu = \int_0^x K_\nu\, \mathrm{d}y$$

The absorption and source functions used in these expressions are the sum of all radiative contributions at ν.

Absorption coefficients derived from either theory or experiment are normally expressed as the product of the absorbing state number density and a radiative cross section

$$K_{\nu_{pc}} = N_p\sigma_{pc}(\nu)$$

or by assuming a Boltzmann distribution exists between the electronic states

$$(K_{\nu_{pc}})_{\mathrm{LTE}} = N_{\mathrm{N}}\left[\frac{g_pe^{-E_p/kT_e}}{Q_{\mathrm{N}}}\sigma_{pc}(\nu)\right] = N_{\mathrm{N}}\sigma'_{pc}(\nu)$$

Thus, an absorption coefficient using the actual state number density N_p can be obtained from one calculated assuming LTE by

$$K_{\nu_{pc}} = \frac{N_p}{(N_p)_{\mathrm{LTE}}}(K_{\nu_{pc}})_{\mathrm{LTE}}$$

where

$$\frac{N_p}{(N_p)_{\mathrm{LTE}}} = \frac{N_p}{N_{\mathrm{N}}}\frac{Q_{\mathrm{N}}}{g_pe^{-E_p/kT_e}}$$

It is desired to have the LTNE corrections in terms of the known number density populations, N_g and N^*. If state p is one of the low-lying states, and since we have assumed these states are in LTE with each other

$$N_p = N_g \frac{g_p e^{-E_p/kT_e}}{Q_{N_g}}$$

$$\frac{N_p}{(N_p)_{\rm LTE}} = \frac{N_{N_g}}{N_N}\frac{Q_N}{Q_{N_g}} = \frac{N_{N_g}}{(N_{N_g})_{\rm LTE}}$$

Similarly, if p is one of the excited states

$$N_p = {\rm N}^*\{g_p \exp[-(E_p - E_4)/kT_E]/Q_{{\rm N}^*}\}$$

$$\frac{N_p}{(N_p)_{\rm LTE}} = \frac{N_{{\rm N}^*}}{N_{\rm N}}\frac{Q_{\rm N}}{Q_{{\rm N}^*}e^{-E_4/kT_e}} = \frac{N_{{\rm N}^*}}{(N_{{\rm N}^*})_{\rm LTE}}$$

The absorption coefficient for atomic line radiation is similar in form to that for the continuum process, but uses a radiative cross section which is a function of both the absorbing, p, and the emitting state, q

$$K_{\nu_{pq}} = N_p \sigma_{pq}(\nu)$$

However, since the number density dependence is only with the absorbing state, the LTNE corrections described above for continuum radiation also apply to the line radiation.

The source function at thermodynamic equilibrium is equal to B_ν

$$(S_{\nu_{pc}})_{\rm LTE} = (S_{\nu_{pq}})_{\rm LTE} = B_\nu = \frac{2h\nu^3}{c^2}(e^{h\nu/kT_e} - 1)$$

The source function for atomic continuum processes under LTNE conditions is given by[18,19]

$$S_{\nu_{pc}} = \frac{(N_p)_E}{N_p}\frac{2h\nu^3}{c^2}\left[e^{h\nu/kT_e} - \frac{(N_p)_E}{N_p}\right]^{-1}$$
$$= \frac{(N_p)_E}{N_p}\frac{e^{h\nu/kT_e} - 1}{e^{h\nu/kT_e} - [(N_p)_E/N_p]}(S_{\nu_{pc}})_{\rm LTE}$$

where the subscript E indicates a number density for state p calculated by assuming that state is in thermodynamic equilibrium with the free electrons and ions. Thus, if I is the ionization energy

$$(N_p)_E = N_{{\rm N}^+}N_e\{g_p \exp[-(E_p - I)/kT_e]/Q_{{\rm N}^+}Q_e\}$$

It can further be observed that when p is a low-lying state $e^{h\nu/kT_e} >> (N_p)_E/N_p$ and $e^{h\nu/kT_e} >> 1$ while for the highly excited states, $(N_p)_E/N_p \simeq 1$. Thus

$$S_{\nu_{pc}} \simeq [(N_p)_E/N_p](S_{\nu_{pc}})_{\rm LTE}$$

As before, the LTNE correction can be written in terms of the known number densities so that if p is one of the ground states

$$\frac{(N_p)_E}{N_p} = \frac{N_{{\rm N}^+}N_e}{N_{N_g}}\frac{Q_{N_g}e^{I/kT_e}}{Q_{{\rm N}^+}Q_e} = \frac{(N_{N_g})_E}{N_{N_g}}$$

while if p is an excited state

$$\frac{(N_p)_E}{N_p} = \frac{N_{{\rm N}^+}N_e}{N_{{\rm N}^*}}\frac{Q_{{\rm N}^*}\exp[(I - E_4)/kT_e]}{Q_{{\rm N}^+}Q_e} = \frac{(N_{{\rm N}^*})_E}{N_{{\rm N}^*}}$$

The source function for the radiative transition from state q to state p under LTNE conditions is[18,19]

$$S_{\nu_{pq}} = \frac{N_q}{N_p}\frac{(N_p)_{\rm LTE}}{(N_q)_{\rm LTE}}\frac{2h\nu^3}{c^2}\left(e^{h\nu/kT_e} - \frac{N_q}{N_p}\frac{(N_p)_{\rm LTE}}{(N_q)_{\rm LTE}}\right)^{-1}$$
$$= \frac{N_q}{N_p}\frac{(N_p)_{\rm LTE}}{(N_q)_{\rm LTE}}\frac{e^{h\nu/kT_e} - 1}{e^{h\nu/kT_e} - (N_q/N_p)[(N_p)_{\rm LTE}/(N_q)_{\rm LTE}]}(S_{\nu_{pq}})_{\rm LTE}$$

If the transition is between two excited states, since it has been assumed that these states are in thermodynamic equilibrium, the LTNE source function becomes identical to that for LTE. If the transition is between an excited state and a ground state, it can be approximated that $e^{h\nu/kT_e} >> 1$ and $e^{h\nu/kT_e} >> N_q(N_p)_{\rm LTE}/N_p(N_q)_{\rm LTE}$ so that it is approximately true that

$$S_{\nu_{pq}} = \frac{N_q}{N_p}\frac{(N_p)_{\rm LTE}}{(N_q)_{\rm LTE}}(S_{\nu_{pq}})_{\rm LTE}$$
$$= \frac{N_{{\rm N}^*}}{N_{N_g}}\frac{(N_{N_g})_{\rm LTE}}{(N_{{\rm N}^*})_{\rm LTE}}(S_{\nu_{pq}})_{\rm LTE}$$

Discussion of Results

Several sets of results have been obtained using the models presented in the previous sections. In all cases, these results are for the stagnation streamline on a vehicle having a 2.3-m nose radius, utilize 99 points between the wall and shock front, and use a nitrogen freestream. For those cases which assume that excited electronic states are in equilibrium with the free ions and electrons, the nonequilibrium chemistry is shown on Table 1. For those cases utilizing the second-order local thermodynamic nonequilibrium model for atoms, the corresponding nonequilibrium chemistry model is shown on Table 2. In addition, the wall has been assumed to be radiatively black, noncatalytic to atomic recombination, fully catalytic to ionic recombination, and at a temperature of 1650 K. This wall temperature was selected to insure significant cool wall thermal effects and is representative of the maximum temperature of nonablating surfaces. However, it is recognized that for the higher speed case considered, the cumulative head load associated with the mission profile dictates the use of ablative

Table 1 Reaction system for first-order LTNE model

Reaction	A	B	E
$N_2 + N = 2N + N$	4.085×10^{22}	−1.5	113,100
$N_2 + N_2 = 2N + N_2$	4.70×10^{17}	−0.5	113,100
$N_2 + e^- = 2N^+ + e^-$	3.00×10^{24}	−1.6	113,100
$N_2 + N^+ = N_2^+ + N$	1.00×10^{12}	0.5	12,200
$N + N = N_2^+ + e^-$	1.40×10^{13}	0.0	67,800
$N + e^- = N^+ + 2e^-$	4.16×10^{13}	0.5	120,000
$N + N = N + N^+ + e^-$	2.34×10^{11}	0.5	120,000
$N + N^+ = 2N^+ + e^-$	2.34×10^{11}	0.5	120,000

Rates in the form $k_f = AT^B \exp(-E/T)$. $T = T_e$ in electron impact reactions.

Table 2 Reaction system for second-order LTNE model

Reaction	A	B	E
$N_2 + N = 2N_g + N$	4.085×10^{22}	−1.5	113,100
$N_2 + N_2 = 2N_g + N_2$	4.70×10^{17}	−0.5	113,100
$N_2 + N^+ = 2N_g + N^+$	1.90×10^{17}	−0.5	113,100
$N_2 + e^- = 2N^+ + e^-$	3.00×10^{24}	−1.6	113,100
$N_2 + N^+ = N_2^+ + N_g$	1.00×10^{12}	0.5	12,200
$N_g + N_g = N_2^+ + e^-$	1.40×10^{13}	0.0	67,800
$N_g + N = N + N^+ + e^-$	2.34×10^{11}	0.5	120,000
$N_g + N^+ = 2N^+ + e^-$	2.34×10^{11}	0.5	120,000
$N_g + e^- = N^+ + 2e^-$	2.50×10^{16}	0.0	169,000
$N_g + e^- = N^* + e^-$	5.56×10^{16}	0.0	121,000
$N^* + e^- = N^+ + 2e^-$	4.11×10^{17}	0.0	48,900

Rates in the form $k_f = AT^B \exp(-E/T)$. $T = T_e$ in electron impact reactions. $N = N_g + N^*$.

surfaces and higher wall temperatures. Finally, an approximate boundary condition representing the wall sheath effects on electrons has been utilized as discussed in Ref. 2. Since the VSL flowfield method uses shock fitting, shock slip boundary conditions have been used for all cases in order to properly conserve total energy.

To investigate the thermal, diffusion, and radiation models, two entry conditions have been considered. The first, sometimes referred to as "AFE CFD Point 4," corresponds to a "max Q" point for an AFE vehicle at which the freestream conditions are 9.326 km/s, 26.4 dyne/cm^2, and 200 K; while the second point is for the same vehicle but at 14 km/s and 80-km altitude. The latter is typical of a Mars return vehicle at an altitude where nonequilibrium phenomena could be significant. All of the 14 km/s cases considered were calculated with radiative-gasdynamic coupling included. Since the AFE cases do not have significant radiative coupling, the radiation calculations have been made from the converged solutions. All radiation calculations have been made with LTNE effects accounted for using the molecular model, and either the first- or second-order atomic models described previously.

Thermal Nonequilibrium Model

All the results presented in this section were calculated using the constant Lewis number (1.4) diffusional model from Miner and Lewis[20] and the chemical reaction set of Table 1, while radiative LTNE effects were calculated using the first-order model. As a result, the results in this section are comparable to the results presented in Ref. 2, with the important distinction that the two-temperature model used previously assumed $T_v = T_{tr}$, while the cases labeled as two-temperature in this article assume $T_v = T_e$.

The first results presented in Figs. 2 and 3 were obtained using a two-temperature model wherein the electron/electronic and vibrational energies are assumed to be highly coupled and in equilibrium with each other.[11] This effect was achieved computationally by summing the two equations term-by-term and solving together. An alternate and, at least theoretically, identical approach could have been achieved by solving the original equation set, while forcing the electron-vibrational relaxation times τ_e to approach zero.

Figure 2 shows that the AFE CFD 4 case is in chemical and thermal nonequilibrium for almost the entire shock layer and that the chemistry is dissociation dominated, the ionization level being very low. The thermal nonequilibrium is particularly interesting in the region of the wall where $T_v - T_e$ exceed the heavy particle translational temperature. In the wall region, both the ionic and atomic recombinations are dumping energy into the electron and vibrational energies, respectively. It is assumed[1] that ionic recombinations occur primarily by the reverse of the electron-impact ionization reaction and that each recombination adds I to the electron translational energy, while the CVDV model[7,8] assumes that each atomic recombination adds $G_s - e_{v,s} \approx D_s/2 - e_{v,s}$ to the vibrational energy of species s. Since $T_v - T_e$ exceeds T_{tr} in the wall thermal layer, it follows that either or both of the recombination reactions is adding energy faster that the translational-vibrational and translational-electron exchange processes can remove it. The maximum value reached by the $T_v - T_e$ temperature was 8515 K at y/yshock = 0.83.

Unlike the AFE CFD 4 case, the 14 km/s case shown in Fig 3. shows a pronounced peak in the $T_v - T_e$ profile of about 17,000 K at 0.83. Both thermal and chemical equilibrium occur for this case at about 0.70, although, due to radiative cooling, the temperature continues to drop after this point along with gradual changes in the chemical composition. While the AFE CFD 4 point was dominated by dissociation, at this speed dissociation occurs very rapidly behind the shock front and ionization processes dominate most of the flow, reaching a peak degree of ionization of about 35%.

Results with the full three-temperature model without electron-vibrational coupling are shown in Figs. 4 and 5. These cases represent the other extreme relative to the two-temperature cases since there is no direct energy exchange mechanism between the electrons and the vibrational states. Indirectly, some energy exchange still occurs through the coupling of both T_e and T_v to T_{tr}.

Comparing the three-temperature results of Fig. 4 with the two-temperature results of Fig. 2, it is seen that except for a greatly different T_e profile, the profiles are very similar. The vibrational temperature does peak a little sooner and higher at the shock front for the three-temperature model, 9100 K

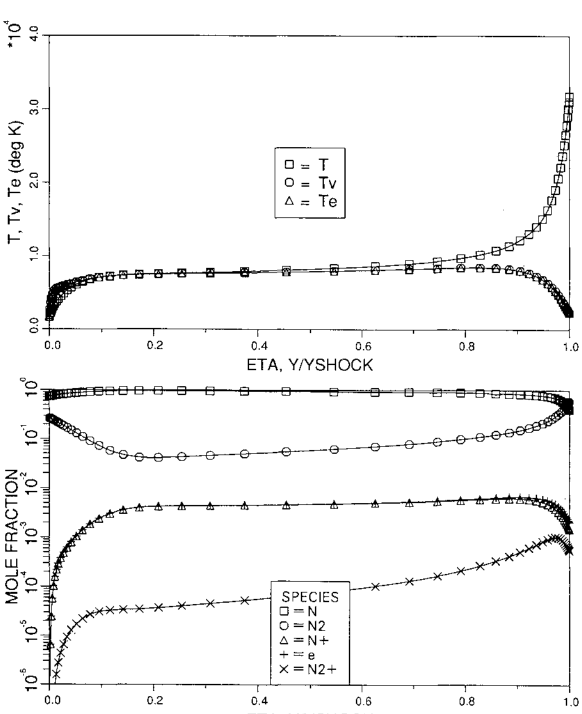

Fig. 2 Stagnation profiles for AFE CFD point 4 two-temperature model, QR = 2.51 W/cm^2, QC = 27.6 W/cm^2, YSHOCK = 13.1 cm.

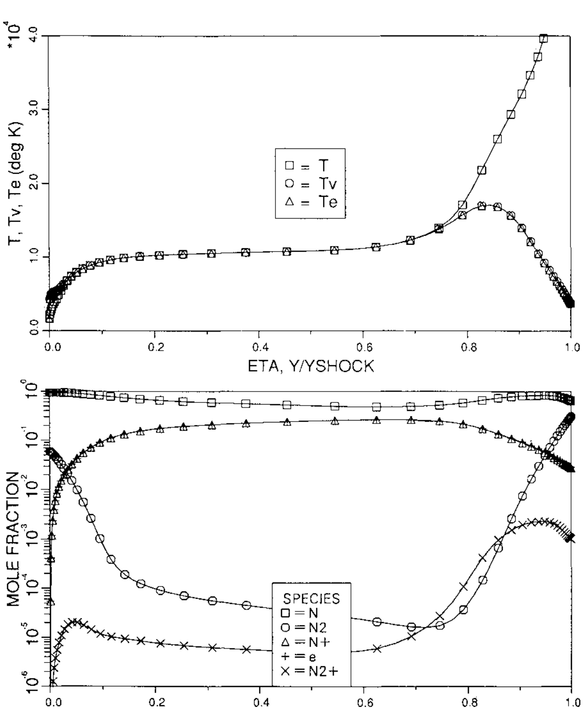

Fig. 3 Stagnation profiles for 14 km/s case two-temperature model, QR = 115.9 W/cm^2, QC = 66.2 W/cm^2, YSHOCK = 9.69 cm.

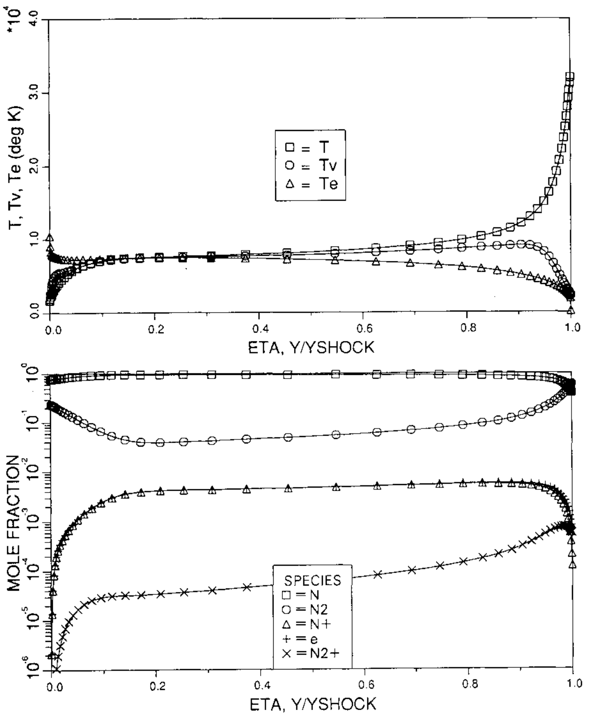

Fig. 4 Stagnation profiles for AFE CFD point 4 three-temperature model, without T_v − T_e coupling, QR = 1.02 W/cm^2, QC = 26.0 W/cm^2, YSHOCK = 13.1 cm.

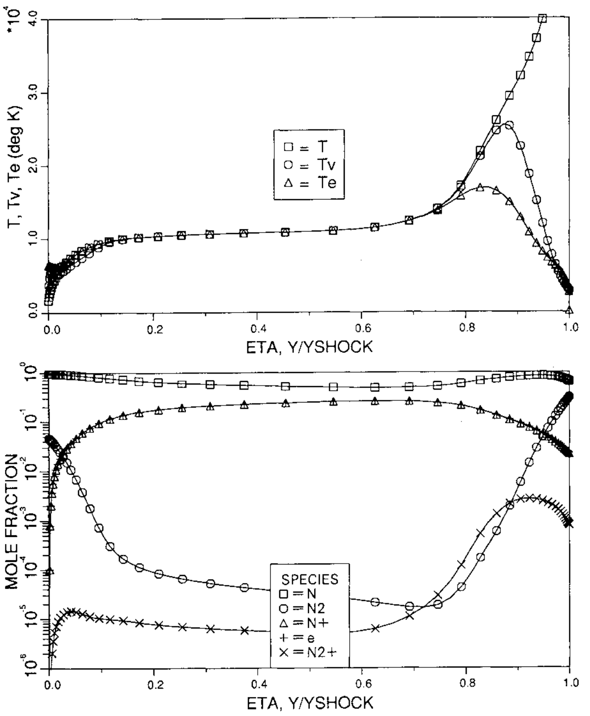

Fig. 5 Stagnation profiles for 14 km/s case three-temperature model, without T_v − T_e coupling, QR = 98.2 W/cm^2, QC = 61.2 W/cm^2, YSHOCK = 9.77 cm.

at 0.91, but has the same profile over the rest of the shock layer, including the overshoot in the thermal boundary layer. Without T_e coupling, this high T_v indicates that energy production due to atomic recombinations is significant in the wall region, as has been seen by other investigators.[21] As a result of electron energy depletion through electron impact ionization, the electron temperature is much lower behind the shock front for this model than before, which results in a much lower radiative heat flux. Also, the lower electron temperature and its effect on the electron impact ionization rate increases the amount of chemical nonequilibrium at the shock front, and in turn, slightly increases the shock standoff distance.

As can be seen from the T_e profile, a shock slip condition was not enforced for the electron/electronic equation. Numerical problems with the slip boundary condition, coupled with the small magnitude of electron number density, have not yet been resolved. This omission, however, does not have a significant effect on the other flow properties since the electron heat conduction is very small at the shock and also does not have a strong effect on the T_e profile itself. The electron temperature solution appears to be uncoupled from the shock boundary condition. This result is consistent with the quasi-equilibrium electron formulation previously used by the authors[1,2] in which it was assumed that chemical energy production and collisional energy transfer dominate the other terms in the electron energy equation, and that T_e is primarily determined by the balance of the two.

The 14 km/s case shown in Fig. 5, when compared with Fig. 3, shows the exact opposite trends as were noticed for the AFE CFD 4 case. The T_e profile is very similar in shape to the T_v − T_e profile, while T_v is greatly different. The vibrational temperature peaks much higher, 23,000 K at 0.86, and equilibrates sooner with T_{tr}, due to high translational coupling. T_e peaks only slightly lower at 16,900 K and 0.82, and as a result there is a slightly lower radiative flux.

In the thermal layer, the three-temperature T_v initially dips below T_{tr} before rising above near the wall as in the two-temperature case. Without electron coupling, diffusive effects in the thermal layer are important in the vibrational energy equation, and the flux of cool N_2 particles away from the wall lowers the vibrational energy until the atomic recombination reactions occur rapidly enough to raise T_v. This diffusive cooling effect was not seen in the AFE CFD 4 case due to the lower concentration gradients in N_2 and thus lower diffusive flux. The electron temperature in the thermal layer shows the same trends as were noted for the two-temperature case.

Figures 6 and 7 show results for the AFE CFD 4 and 14 km/s cases, respectively, where the three-temperature model is used with electron-vibrational coupling, as described previously in the theory section. As might be expected, these results are in-between the two extreme cases of the two-temperature model and the three-temperature model without T_v − T_e coupling. In the AFE CFD 4 case, the electron temperature has been increased toward T_v in the shock front, equilibrates with it around 0.70, and stays in equilibrium through the rest of the shock layer except for a slight divergence immediately off the wall. The higher T_e profile results in a factor of two larger radiative flux than the uncoupled T_v − T_e case, but it is still lower than the two-temperature case.

For the 14 km/s case, T_v − T_e coupling lowers the vibrational temperature in the shock front region (from a peak value of 23,000 K to 22,200 K) while slightly raising the T_e profile, and reduces the amount of diffusional cooling of T_v in the wall thermal layer. Percentage-wise, the two-temperature assumption has a slightly greater effect on the radiative flux for the lower speed case than the higher, 30% compared to 20%. The percentage differences would be further apart for the two cases if it were not for the fact that LTNE corrections tend to reduce the amount of radiation from the thermal nonequilibrium regions.

Second-Order Atomic LTNE Model

The results in this final section are cases which used the full diffusional model of Ref. 3, the chemical reaction rates of Table 2, and the second-order atomic LTNE model discussed in the theory section of this article. Results obtained using full diffusional model do not differ significantly from those from the binary model in a nitrogen freestream[3] and should not effect the following observations. The AFE CFD 4 results shown in Fig. 8 are very close to the previous results shown in Fig. 6. The only significant difference is in the N^+

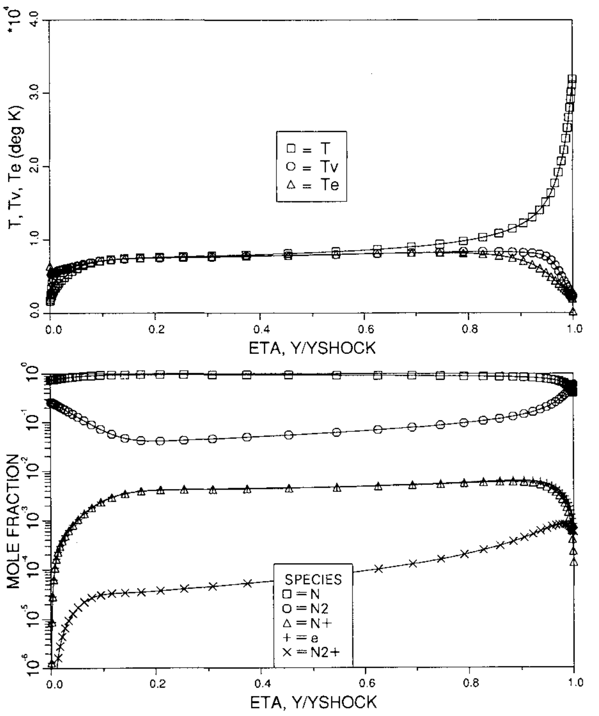

Fig. 6 Stagnation profiles for AFE CFD point 4 three-temperature model, with $T_v - T_e$ coupling, QR = 1.93 W/cm^2, QC = 27.2 W/cm^2, YSHOCK = 13.1 cm.

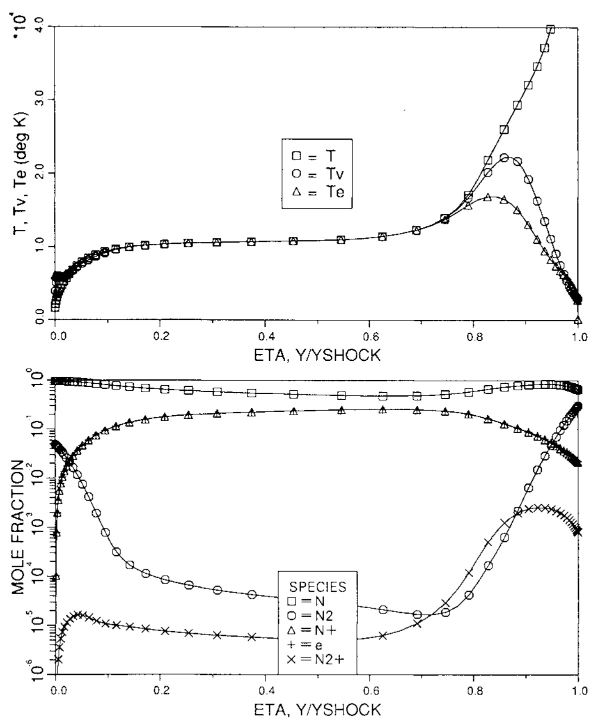

Fig. 7 Stagnation profiles for 14 km/s case three-temperature model, with $T_v - T_e$ coupling, QR = 97.7 W/cm^2, QC = 59.9 W/cm^2, YSHOCK = 9.77 cm.

and N_2^+ profiles at the shock front. The new rate for excitation of N is faster than the rate in Table 1 which leads to a faster total ionization rate even though the ionization from the excited states is not infinite. As a result of this faster ionization rate, there is a higher concentration of N^+ near the shock; and as a result of the charge exchange reaction and ambipolar diffusion effects, the higher N^+ concentration in turn slightly lowers the N_2^+ concentration. The calculated N^* population is very low and closely follows the T_e profile in detail as can partially be seen from the figure.

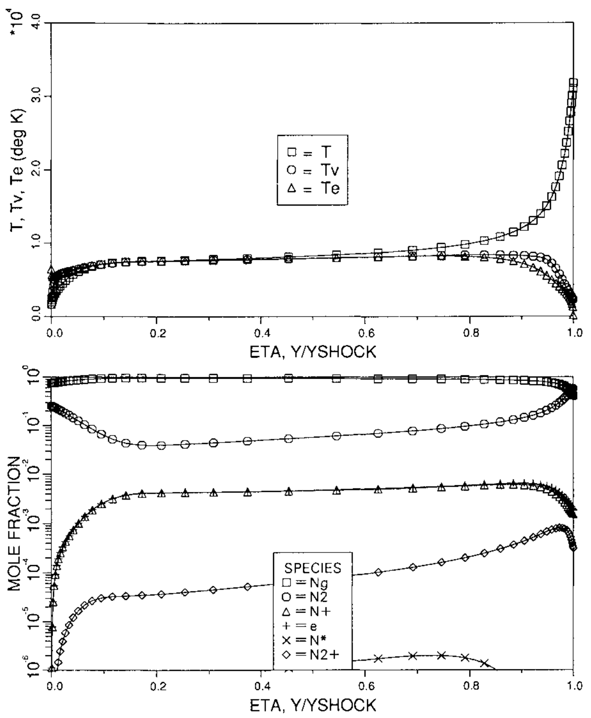

Fig. 8 Stagnation profiles for AFE CFD point 4 second-order LTNE model, QR = 2.38 W/cm^2, QC = 27.8 W/cm^2, YSHOCK = 13.1 cm.

This case can also be compared to the similar case results presented in Ref. 2. The total radiation calculated in Ref. 2 is lower than the current results, due primarily to a lower T_e temperature calculated by the quasiequilibrium electron/electronic energy equation used in Ref. 2. The radiative spectral differences between the previous case and this present case, however, should be due to the differences in the first- and second-order LTNE correction methods. The radiative spectral details of the radiation reaching the wall for the AFE CFD 4 case are shown in Fig. 9 in two forms; the first shows the atomic line radiation having been grouped into convenient blocks while the second shows the atomic lines in full detail. Having the lines grouped gives a better visual description of the magnitude of the relative radiative process, whereas the detailed presentation bears more similarity to experimental results.

While the radiation shown in Fig. 9 is still dominated by the $N_2^+(1-)$ molecular band in the 2–4 eV range, these new results show a much larger contribution from atomic lines in both the infrared (IR) and ultraviolet (UV) regions, especially in the IR region. In fact, the first-order LTNE results from Ref. 1 showed almost no atomic radiation at all due to the large region of LTNE predicted for this case. The second-order LTNE model predicts less LTNE for line radiation since the excited atomic electronic energy states are not as depleted as before.

The 14 km/s case shown in Fig. 10 exhibits significant differences from the results in Fig. 7. The higher nitrogen excitation rate in Table 2 has shortened the nonequilibrium region at the shock front and lowered the peak T_e from 16,650 K to 14,560 K. Since this case is dominated by ionization chemistry, it would be expected that the results are sensitive to the ionization/excitation rates. The group and detailed wall radiation spectral plots are given as Fig. 11. Atomic radiation dominates for this case and most of it comes from the continuum UV bands. Strongly emitting IR lines are still seen, and the high UV lines above 11 eV are highly absorbed at the lines' centers.

Rather than compare these results to the earlier results which are greatly different in the chemical and thermal profiles, it was decided to recalculate the results of Fig. 7 using

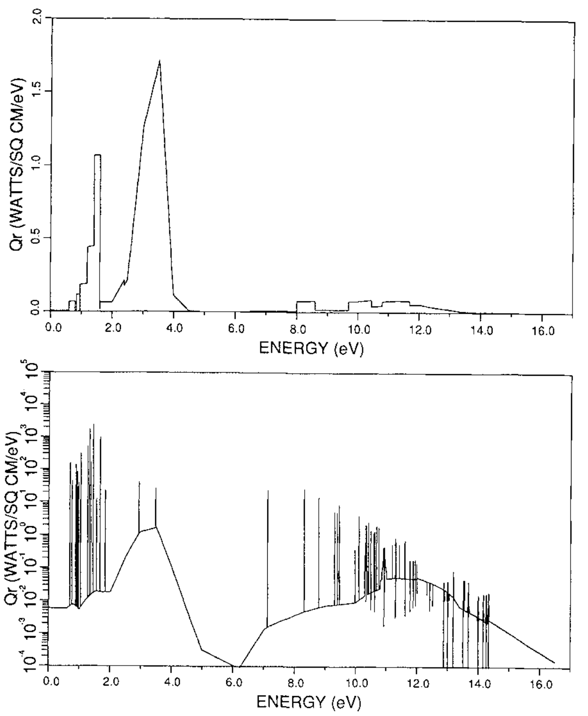

Fig. 9 Spectral radiation profiles for AFE CFD point 4, second-order LTNE model.

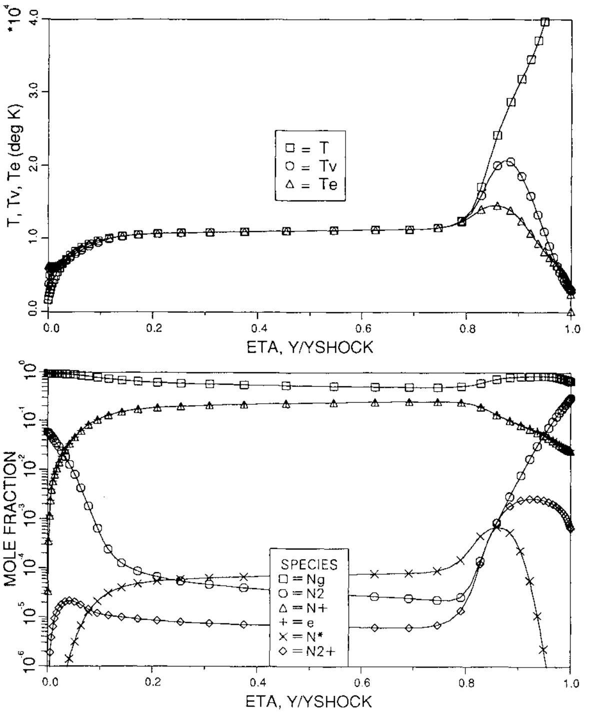

Fig. 10 Stagnation profiles for 14 km/s case second-order LTNE model, *QR* = 89.0 W/cm², *QC* = 55.1 W/cm², YSHOCK = 9.59 cm.

the higher excitation rate for N in place of the electron impact rate in Table 1. In this manner, first-order LTNE results could be obtained with a chemical model very similar to that for the second-order LTNE method. The flowfield profiles for this case are shown in Fig. 12. As expected, these profiles are very similar to those of Fig. 10 except that the peak T_e is lower, 13,860 K, and equilibrium occurs slightly sooner. The earlier equilibration is to be expected since the first-order LTNE assumes instantaneous equilibration of the excited states with the ions and electrons, while the second-order has a finite rate.

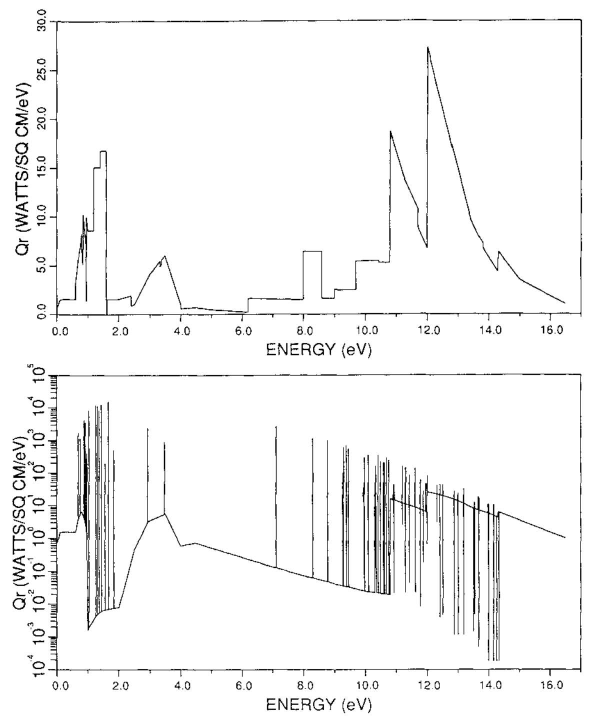

Fig. 11 Spectral radiation profiles for 14 km/s case, second-order LTNE model.

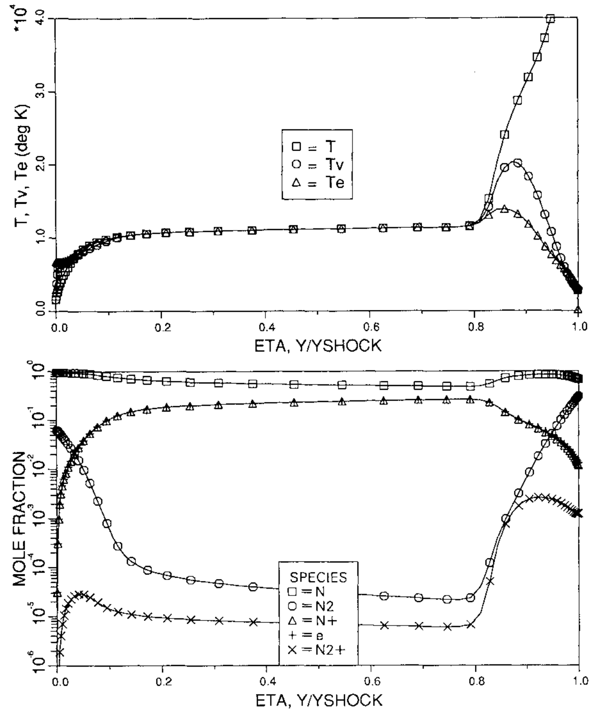

Fig. 12 Stagnation profiles for 14 km/s case first-order LTNE model with new excitation rate, *QR* = 82.2 W/cm², *QC* = 54.3 W/cm², YSHOCK = 9.58 cm.

The radiative spectral plots for this case are shown in Fig. 13. In comparing these results to those in Fig. 11, three important differences are noticed. First, the IR line radiation is enhanced in the second-order model over the first-order model. This greater amount of emission is due to the lower level of thermodynamic nonequilibrium predicted from the second-order method. The first-order method predicts a largely depleted excited state population in the peak T_e region, which reduces the line radiation from this region. Also, because of the reduced line radiation, absorption of the UV lines in the

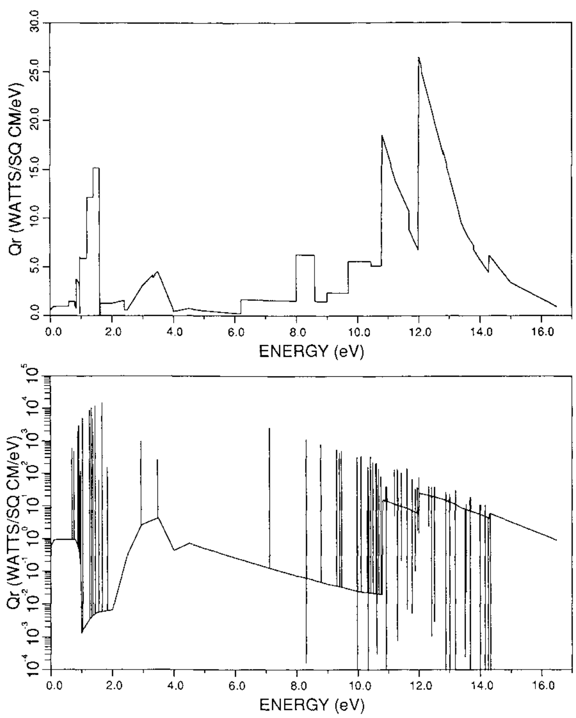

Fig. 13 Spectral radiation profiles for 14 km/s case first-order LTNE model with new excitation rate.

wall-boundary layer is more significant for the first-order LTNE model than for the second-order model. The difference in UV line center absorption is the second noticeable difference between Figs. 13 and 11. Finally, the N_2^+ (1-) molecular band is larger for the second-order LTNE model. This difference appears to be due to a number of subtle changes in the two flowfields such as different radiative cooling effects and different N_2^+ number densities caused by the charge exchange chemical reaction.

Conclusions

The use of a three-temperature model including electron-vibrational coupling can lead to significant differences in the thermal profiles from those obtained with a two-temperature model. The effects on chemistry are not as noticeable due to the fact that the combined $T_v - T_e$ model tends to predict a temperature closest to the dominant energy for the flow conditions, i.e., closer to T_v in dissociation dominated flows, and closer to T_e in ionization dominated flows. The differences in the thermal profiles for the two models results in differences of 20–30% in the radiative heat flux to the wall for the cases considered. These radiative differences would be more significant except that LTNE effects tend to inhibit emission from the regions of thermal nonequilibrium.

The second-order LTNE model developed for this article has shown deficiencies in the first-order LTNE model. While both models predict similar total heat fluxes, the spectral content of the radiation is different. Radiation reaching the wall with the second-order LTNE model shows a greater IR line contribution and less UV line center absorption. The electron impact excitation calculated for the second-order LTNE model is faster by an order of magnitude than the previous current rate. Using this faster rate with the first-order model can closely reproduce much of the chemical behavior of the second-order model.

Acknowledgments

This work was primarily supported by NASA Grant NAG-1-1003 from the Langley Research Center, with Lin C. Hartung as technical monitor. T. A. Gally is partially supported by a NASA Graduate Student Researchers Fellowship through the NASA Johnson Space Center.

References

[1]Carlson, L. A., and Gally, T. A., "The Effect of Electron Temperature and Impact Ionization on Martian Return AOTV Flowfields," AIAA Paper 89-1729, June 1989.

[2]Carlson, L. A., and Gally, T. A., "Nonequilibrium Chemical and Radiation Coupling Phenomena in AOTV Flowfields," AIAA Paper 91-0569, Jan. 1991.

[3]Gally, T. A., Carlson, L. A., and Green, D., "A Flowfield Coupled Excitation and Radiation Model for Nonequilibrium Reacting Flows," AIAA Paper 91-1463, June 1991.

[4]Thompson, R. A., "Comparison of Nonequilibrium Viscous Shock Layer Solutions with Windward Surface Shuttle Heating Data," AIAA Paper 87-1473, June 1987.

[5]Nicolet, W. E., "User's Manual for the Generalized Radiation Transfer Code (RAD/EQUIL or RADICAL)," NASA CR 116353, Oct. 1969.

[6]Park, C., *Nonequilibrium Hypersonic Aerothermodynamics*, Wiley, New York, 1990, pp. 166, 167.

[7]Treanor, C. E., and Marrone, P. V., "Effect of Dissociation on the Rate of Vibration Relaxation," *Physics of Fluids*, Vol. 5, No. 9, 1962, pp. 1022–1026.

[8]Marrone, P. V., "Inviscid, Nonequilibirum Flow Behind Bow and Normal Shock Waves, Part I.—General Analysis and Numerical Examples," Cornell Aeronautical Lab. Rept. QM-1626-a-12(I), Buffalo, NY, May 1963.

[9]Park, C., "Calculation of Nonequilibrium Radiation in the Flight Regimes of Aeroassisted Orbital Transfer Vehicles," *Thermal Design of Aeroassisted Orbital Transfer Vehicles*, edited by H. F. Nelson, Vol. 96, Progress in Astronautics and Aeronautics, AIAA, New York, 1985, pp. 395–418.

[10]Millikan, R. C., and White, D. R., "Systematics of Vibrational Relaxation," *Journal of Chemical Physics*, Vol. 39, No. 12, 1963, pp. 3209–3213.

[11]Park, C., "Assessment of Two Temperature Kinetic Model for Ionizing Air," AIAA Paper 87-1574, June 1987.

[12]Lee, J. H., "Electron-Impact Vibrational Excitation Rates in the Flowfield of Aeroassisted Orbital Transfer Vehicles," *Thermophysical Aspects of Re-entry Flows*, edited by J. N. Moss and C. D. Scott, Vol. 103, Progress in Astronautics and Aeronautics, AIAA, New York, 1986, pp. 197–224.

[13]Candler, G. and Park, C., "The Computation of Radiation from Nonequilibrium Hypersonic Flows," AIAA Paper 88-2678, June 1988.

[14]Carlson, L. A., Bobskill, G. J., and Greendyke, R. B., "Comparison of Vibration Dissociation and Radiative Transfer Models for AOTV/AFE Flowfields," *Journal of Thermophysics and Heat Transfer*, Vol. 4, No. 1, 1990, pp. 16–26.

[15]Kunc, J. A., and Soon, W. H., "Collisional Radiative Nonequilibrium in Partially Ionized Atomic Nitrogen," *Physical Review A*, Vol. 40, No. 10, 1989, pp. 5822 ff.

[16]Foley, W. H., and Clarke, J. H., "Shock Waves Structured by Nonequilibrium Ionizing and Thermal Phenomena," *Physics of Fluids*, Vol. 16, No. 3, 1973, pp. 1612–1620.

[17]Nelson, H. F., "Nonequilibrium Structure of Argon Shock Waves," *Physics of Fluids*, Vol. 16, No. 12, 1973, pp. 2132–2142.

[18]Chapin, C. E., "Nonequilibrium Radiation and Ionization in Shock Waves," AA&ES Rept., Purdue Univ., Lafayette, IN, June 1967.

[19]Clarke, J. H., and Ferrari, C., "Gas Dynamics with Nonequilibrium Radiative and Collisional Ionization," *Physics of Fluids*, Vol. 8, No. 12, 1965, pp. 2121–2139.

[20]Miner, E. W., and Lewis, C. H., "Hypersonic Ionizing Air Viscous Shock Layer Flows over Nonanalytic Blunt Bodies," NASA CR-2550, May 1975.

[21]Gnoffo, P. A., Gupta, R. N., and Shinn, J. L.," Conservation Equations and Physical Models for Hypersonic Air Flows in Thermal and Chemical Nonequilibrium," NASA TP 2867, Feb. 1987.